Normative Measurements of the Chinese Extraocular Musculature by High-Field Magnetic Resonance Imaging

Sunny Shen,[1,2] *Kee Siew Fong,*[1,2] *Hwee Bee Wong,*[3] *Audrey Looi,*[1,2] *Ling Ling Chan,*[4] *Jack Rootman,*[5] *and Lay Leng Seah*[1,2]

Purpose. To establish the normal measurements of diameter and cross-sectional area of the Chinese extraocular muscles (EOMs) and optic nerve-sheath complex (ON) as seen on high-field (3-Tesla; 3T) magnetic resonance imaging (MRI).

Methods. Coronal 3T MRI of the orbit (TR, 700 ms; TE, 15 ms; FOV, 160 mm; matrix, 256 × 256; slice thickness, 1 mm; and slice gap, 0) was performed on 80 normal Chinese volunteers. T1-weighted images were analyzed with computer-assisted segmentation. The diameter and the cross-sectional area of EOMs and the ON were measured from the image plane at the posterior aspect of the globe and at 7 mm behind the globe. The maximum diameter of EOM was measured from their respective reconstructed images.

Results. The normal measurement (mean ± SD) of diameter at the posterior aspect of the globe: medial rectus (MR), 3.6 ± 0.4 mm; inferior rectus (IR), 3.7 ± 0.8 mm; lateral rectus (LR), 2.3 ± 0.5 mm; superior oblique (SO), 2.4 ± 0.6 mm; and the ON, 5.4 ± 0.7 mm. The normal measurement of diameter 7 mm behind the globe: MR, 3.2 ± 0.6 mm; IR, 3.9 ± 0.8 mm; LR, 4.0 ± 0.8 mm; SO, 2.2 ± 0.7 mm; and ON, 4.2 ± 0.5 mm. The normal measurement of cross-sectional area at the posterior aspect of the globe: superior muscle group (SMG), 28.2 ± 6.5 mm^2; MR, 25.5 ± 3.2 mm^2; IR, 26.9 ± 7.2 mm^2; LR, 17.3 ± 3.9 mm^2; SO, 10.5 ± 3.5 mm^2; and ON, 27.6 ± 6.1 mm^2. The normal measurement of cross-sectional area 7 mm behind the globe: SMG, 24.1 ± 6.6 mm^2; MR, 19.1 ± 4.6 mm^2; IR, 29.5 ± 6.6 mm^2; LR, 32.3 ± 6.5 mm^2; SO, 9.7 ± 3.9 mm^2; and ON, 17.1 ± 2.9 mm^2. The normal measurement of maximum diameter: SMG, 4.8 ± 1.1 mm; MR, 5.1 ± 0.9 mm; IR, 5.4 ± 1.0 mm; and LR, 4.5 ± 0.9 mm.

Conclusions. The Chinese 3T MRI EOMs and ON normative data may be useful in determining pathologic enlargement of the EOMs and ON in various orbital conditions. (ClinicalTrials .gov number, NCT00348413.) (*Invest Ophthalmol Vis Sci.* 2010;51:631–636) DOI:10.1167/iovs.09-3614

From the [1]Singapore National Eye Centre, Singapore; the [2]Singapore Eye Research Institute, Singapore; the [3]Clinical Trials and Epidemiology Research Unit, Singapore; the [4]Department of Diagnostic Radiology, Singapore General Hospital, Singapore; and the [5]Department of Ophthalmology and Visual Sciences, University of British Columbia, Vancouver, British Columbia, Canada.

Supported by Biomedical Research Council (BMRC) Grant R272/16/2002, Singapore.

Submitted for publication February 24, 2009; revised May 10, June 27, and July 16, 2009; accepted July 17, 2009.

Disclosure: **S. Shen**, None; **K.S. Fong**, None; **H.B. Wong**, None; **A. Looi**, None; **L.L. Chan**, None; **J. Rootman**, None; **L.L. Seah**, None

Corresponding author: Lay Leng Seah, Oculoplastic Service, Singapore National Eye Centre, 11 Third Hospital Avenue, Singapore 168751; seah.lay.leng@snec.com.sg.

Magnetic resonance imaging (MRI) has been widely used in the assessment of various orbital conditions. In thyroid orbitopathy (TO), a range of MRI techniques have been developed to study the phases of disease and to monitor its response with treatment: T_2 relaxation time,[1,2] signal intensity in T_2-weighted image (T2-SI),[3] signal intensity ratio (SIR) in short τ inversion recovery (STIR) sequence,[4–7] contrast enhancement pattern,[8–10] and volumetric measurement of the muscles.[11–14] However, all these methods are time consuming and hardware dependent. For everyday management of patients, clinicians need simpler parameters that are easily assessable.

Morphologic parameters of the extraocular muscles (EOMs), the diameters (i.e., thickness and width), and the cross-sectional area, are readily available in any standard MRI scan of the orbit. In several studies, these parameters have been used to monitor TO as an outcome measure for treatment efficacy.[13–16] Szucs-Farkas et al.[15] have shown that the diameters and the cross-sectional area of EOMs correlate well with its volume, a direct but technically demanding parameter in monitoring TO.

For any parameter to be useful clinically, the normal range must be known. Although the computed tomography (CT) and the MRI anatomy of the orbital structures have been well described, only a few studies reported the normative radiologic values,[17–20] and none of these studies focused on a particular ethnic group such as the Chinese population. In this study, we present the normal measurements of diameter and cross-sectional area of EOMs in the Chinese as seen on high-field (3 Tesla; 3T) MRI and the changes in these parameters in relation to age and sex.

Methods

The study protocol was approved by the Institutional Review Board of the Singapore Eye Research Institute, Singapore, registered on ClinicalTrials.gov in the United States, and performed in accordance with the World Medical Association's Declaration of Helsinki. All participants were recruited after written informed consent.

Subjects

One hundred sixty orbits of 80 normal Chinese volunteers were evaluated in the study. Ten men and 10 women were recruited from each of four decades of life: 21 to 30, 31 to 40, 41 to 50, and 51 to 60. All participants had no clinical evidence or history of endocrine disease (e.g., thyroid), orbital disorder, muscular disease, ophthalmic disorder (e.g., myopia >6.0 D, strabismus) or psychological illness (e.g., claustrophobia).

MRI Examination

A 3T MRI system (Magnetom Allegra; Siemens AG, Erlangen, Germany) with a single channel 3T neuroimaging head coil were used for the orbital imaging. The scanner was calibrated periodically to assure standardization.

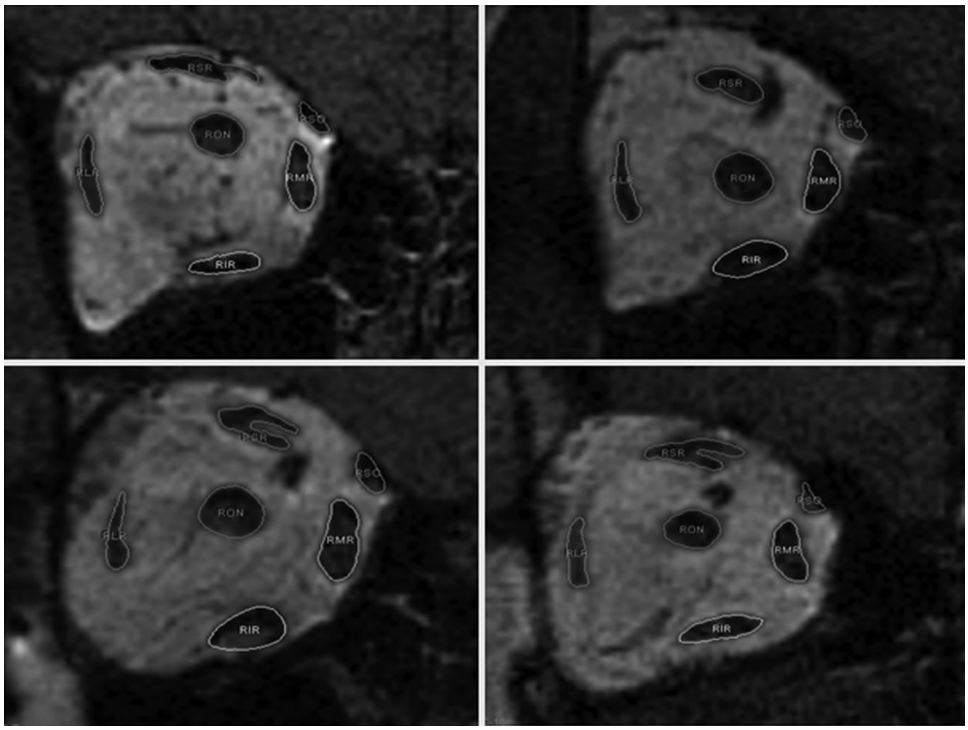

FIGURE 1. Spatial variations of SR and LPS in the SMG of right eye (R) EOMs.

The orbital scan consisted of unenhanced spin-echo T1-weighted coronal acquisition (TR, 700 ms; TE, 15 ms; FOV, 160 mm; matrix, 256 × 256; slice thickness, 1 mm; and slice gap, 0) from the equator of the globe to the orbital apex with the equator and the posterior clinoid process as the anterior and posterior landmarks, respectively. Each scan took approximately 6 minutes.

The examination was performed with each participant lying supine with his or her head stabilized. With the limited space inside the magnet gantry, a distant fixation target was placed with the help of a mirror in the central position to help participants in maintaining primary gaze position throughout the scan. Scout images in the axial, coronal, and sagittal planes were used to ensure optimal head positioning. Participants were instructed to avoid unnecessary movements and to fixate on the distant target. If a motion artifact was detected during the study, the sequence was repeated.

Image Analysis

All image analysis was performed in the Morphometry Unit, Cognitive Science Laboratory, SingHealth Research Facilities, Singapore Health Service, Singapore.

All the MRI data were transferred to a computer (Macintosh; Apple Computer, Cupertino, CA) in the original digital imaging and communications in medicine (DICOM) format. Measurements were taken with biomedical imaging software (Analyze 7.0; AnalyzeDirect, Overland Park, KS) with an interactive pen display (DTU-710; Wacom Corp.,

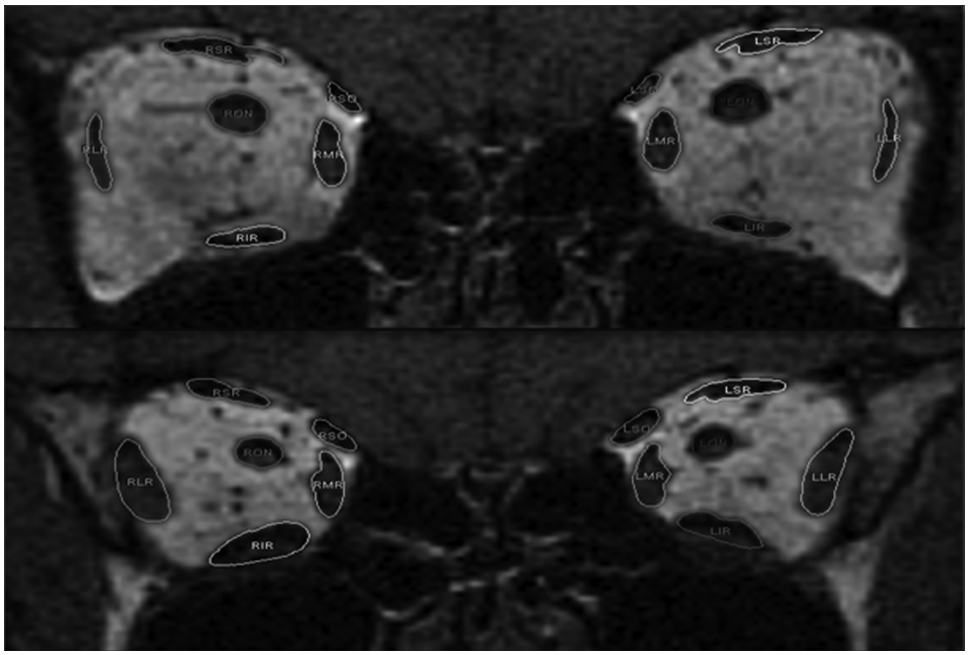

FIGURE 2. The preselected coronal planes at 0 mm behind the globe (*top*) and 7 mm behind the globe (*bottom*) with right (R) and left (L) eye EOMs outlined.

FIGURE 3. The diameter of the EOM was obtained from the thickest part of the muscle that is perpendicular to its long axis.

Saitama, Japan). All the images were reviewed, and only those free of degradation by motion or other artifacts were analyzed.

The superior rectus (SR) and the levator palpebrae superioris (LPS) were difficult to differentiate in MRI, and so they were considered together as the superior muscle group (SMG). In view of their variable anatomic arrangement (Fig. 1), meaningful measurement of diameter was not possible. In this study, we concentrated only on the cross-sectional area and maximum diameter of the SMG.

The following parameters were studied: 1. The diameter (i.e., thickness) of the medial rectus (MR), lateral rectus (LR), inferior rectus (IR), superior oblique (SO), and optic nerve sheath complex (ON). 2. The cross-sectional area of the SMG, MR, LR, IR, SO, and ON on two preselected coronal planes: at the posterior aspect of the globe and 7 mm behind the globle. Before measurement, manual labeling of individual structures on the interactive pen display was performed by selecting the seed signal intensity within. Each EOM and ON was then outlined by adjusting the range of signal intensity in computer-assisted segmentation. Further manual input was necessary to delineate adjacent structures with similar signal intensity (Fig. 2). For EOMs diameter measurement, the longest dimension of each muscle was first established as the long axis, and the diameter reading was taken from the thickest part of the muscle that was perpendicular to it (Fig. 3). For ON thickness measurement, the radiologic vertical diameter of the ON was used. For cross-sectional area measurement, the reading was calculated automatically by the image analysis program once the EOMs and ON were outlined.

3. The maximum diameters (i.e., maximum thicknesses) of the SMG, MR, IR, and LR were determined from their respective reconstructed images. For the MR and LR, the reading was taken from the thickest part of the muscle that was perpendicular to its own course in the axial view. For the SMG and IR, the reading was taken from the thickest part of the muscle that was perpendicular to its course in the quasisagittal view (in line with the intraorbital course of the ON). The precision for all measurements was to the tenths of the unit (i.e., 0.1 mm).

Statistical Analysis

To assess the reliability and the repeatability of our analysis, we calculated inter- and intraobserver reliability. For interobserver reliability, a second independent observer repeated the measurement of 16 randomly selected orbits. For intraobserver reliability, the first observer repeated the measurement of the same 16 orbits after a 3-month interval. Both observers were masked to the participants' demographics (age and sex) and any previous measurements throughout the study.

A paired sample *t*-test was used to compare data between the right and the left orbits. An independent-samples *t*-test was used for the effect of the sex of the subject. Linear regression was used for the effect of age. Multivariable linear regression was used for the effect of both sex and age (all calculations performed with SPSS, ver. 13; SPSS, Chicago, IL). The level of statistical significance was set at $P < 0.05$.

RESULTS

One hundred sixty orbits, 80 right and 80 left, were imaged. There was no statistically significant difference between measurements from the right and the left orbits and only data from the right orbit are reported.

The mean values, standard deviations (SD), and normal ranges (mean ± 2SD) of the diameter, the cross-sectional area, and the maximum diameter of the EOMs and ON were presented in Table 1. The normal measurement (mean ± SD) of diameter at the posterior aspect of the globe was MR, 3.6 ± 0.4 mm; IR 3.7 ± 0.8 mm; LR, 2.3 ± 0.5 mm; SO, 2.4 ± 0.6 mm; and ON, 5.4 ± 0.7 mm. The normal measurement of diameter 7 mm behind the globe was MR, 3.2 ± 0.6 mm; IR, 3.9 ± 0.8 mm; LR, 4.0 ± 0.8 mm; SO, 2.2 ± 0.7 mm; and ON, 4.2 ± 0.5 mm. The normal measurement of cross-sectional area at the posterior aspect of the globe was SMG, 28.2 ± 6.5 mm^2; MR, 25.5 ± 3.2 mm^2; IR, 26.9 ± 7.2 mm^2; LR, 17.3 ± 3.9 mm^2; SO, 10.5 ± 3.5 mm^2; and ON, 27.6 ± 6.1 mm^2. The normal measurement of cross-sectional area 7 mm behind the globe was SMG, 24.1 ± 6.6 mm^2; MR, 19.1 ± 4.6 mm^2; IR, 29.5 ± 6.6 mm^2; LR, 32.3 ± 6.5 mm^2; SO, 9.7 ± 3.9 mm^2; and ON, 17.1 ± 2.9 mm^2. The normal measurement of maximum diameter was SMG, 4.8 ± 1.1 mm; MR, 5.1 ± 0.9 mm; IR, 5.4 ± 1.0 mm; and LR, 4.5 ± 0.9 mm.

There was no consistent statistically significant correlation between measurements and demographic factors (sex and age). In the independent-samples *t*-test, the cross-sectional area of ON and the diameter of IR at the posterior aspect of the globe, was bigger in male participants ($P = 0.024$ and 0.036;

TABLE 1. Normative MRI Measurement of the Chinese Orbits

	Thickness (mm)						Cross-sectional Area (mm^2)						Maximal Thickness (mm)		
	at 0 mm			at 7 mm			at 0 mm			at 7 mm					
Parameter	Mean	SD	Normal Range	Mean	SD	Normal Range	Mean	SD	Normal Range	Mean	SD	Normal Range	Mean	SD	Normal Range
SMG	N/A			N/A			28.2	6.5	15.2–41.2	24.1	6.6	10.9–37.3	4.8	1.1	2.6–7.0
MR	3.6	0.4	2.8–4.4	3.2	0.6	2.0–4.4	25.5	3.2	19.1–31.9	19.1	4.6	9.9–28.3	5.1	0.9	3.3–6.9
IR	3.7	0.8	2.1–5.3	3.9	0.8	2.3–5.5	26.9	7.2	12.5–41.3	29.5	6.6	16.3–42.7	5.4	1.0	3.4–7.4
LR	2.3	0.5	1.3–3.3	4.0	0.8	2.4–5.6	17.3	3.9	9.5–25.1	32.3	6.5	19.3–45.3	4.5	0.9	2.7–6.3
SO	2.4	0.6	1.2–3.6	2.2	0.7	0.8–3.6	10.5	3.5	3.5–17.5	9.7	3.9	1.9–17.5	N/A		
ON	5.4	0.7	4.0–6.8	4.2	0.5	3.2–5.2	27.6	6.1	15.4–39.8	17.1	2.9	11.3–22.9	N/A		

TABLE 2. Normative MRI Measurements of the Chinese Orbits by Sex

		Thickness (mm)						Cross-sectional Area (mm2)						Maximum Thickness (mm)		
		at 0 mm			at 7 mm			at 0 mm			at 7 mm					
Parameter	Sex	Mean	SD	Normal Range	Mean	SD	Normal Range	Mean	SD	Normal Range	Mean	SD	Normal Range	Mean	SD	Normal Range
SMG	M	N/A			N/A			28.6	6.0	16.6–40.6	24.6	6.1	12.4–36.8	4.8	1.0	2.8–6.8
	F	N/A			N/A			27.7	7.1	13.5–41.9	23.6	7.1	9.4–37.8	4.7	1.1	2.5–6.9
P										0.563			0.500			0.701
MR	M	3.6	0.4	2.8–4.4	3.2	0.5	2.2–4.2	25.9	3.3	19.3–32.5	19.4	4.9	9.6–29.2	5.2	0.9	3.4–7.0
	F	3.5	0.5	2.5–4.5	3.2	0.7	1.8–4.6	25.1	3.0	19.1–31.1	18.9	4.4	10.1–27.7	5.0	0.9	3.2–6.8
P				0.154			0.981			0.224			0.606			0.312
IR	M	3.9	0.7	2.5–5.3	3.9	0.7	2.5–5.3	28.3	6.4	15.5–41.1	29.9	6.8	16.3–43.5	5.3	1.0	3.3–7.3
	F	3.5	0.8	1.9–5.1	3.9	0.8	2.3–5.5	25.6	7.6	10.4–40.8	29.1	6.4	16.3–41.9	5.5	1.0	3.5–7.5
P				**0.036**			0.941			0.088			0.620			0.346
LR	M	2.3	0.5	1.3–3.3	3.8	0.9	2.0–5.6	17.6	3.6	10.4–24.8	31.6	7.1	17.4–45.8	4.6	0.9	2.8–6.4
	F	2.3	0.4	1.5–3.1	4.1	0.6	2.9–5.3	16.9	4.1	8.7–25.1	32.9	5.8	21.3–44.5	4.4	0.9	2.6–6.2
P				0.734			0.099			0.404			0.375			0.334
SO	M	2.4	0.5	1.4–3.4	2.2	0.8	0.6–3.8	10.3	3.2	3.9–16.7	9.7	4.1	1.5–17.9	N/A		
	F	2.4	0.7	1.0–3.8	2.1	0.6	0.9–3.3	10.7	3.8	3.1–18.3	9.6	3.8	2.0–17.2	N/A		
P				0.725			0.538			0.576			0.894			
ON	M	5.5	0.7	4.1–6.9	4.3	0.4	3.5–5.1	29.1	6.1	16.9–41.3	17.3	3.0	11.3–23.3	N/A		
	F	5.3	0.7	3.9–6.7	4.1	0.5	3.1–5.1	26.1	5.7	14.7–37.5	16.9	2.8	11.3–22.5	N/A		
P				0.058			0.217			**0.024**			0.549			

Bold probabilities are statistically significant.

Table 2). In the linear regression analysis, the cross-sectional area of LR decreased with age (20.2 mm^2; $P < 0.001$ for age 21–30, 17.4 mm^2; $P = 0.040$ for age 31–40, 16.8 mm^2; $P = 0.010$ for age 41 to 50; and 14.6 mm^2 for age 51–60; Table 3) In the multivariate linear regression analysis, there was no observable trend of correlation of any of the measurements with the demographic factors.

The inter- and intraobserver reliability of most measurements were excellent to perfect, with the intraclass correlation coefficient (ICC) ranging from 0.77 to 1.00. The ICC of four measurements had only moderate to good agreement: thickness of the IR at 0 mm behind the globe (0.47) and the thickness of the IR (0.49; 0.50), LR (0.67; 0.70), and ON (0.71) at 7 mm behind the globe.

TABLE 3. Normative MRI Measurements of the Chinese Orbits by Age

		Thickness (mm)						Cross-sectional Area (mm2)						Maximum Thickness (mm)		
		at 0 mm			at 7 mm			at 0 mm			at 7 mm					
Parameter	Age (y)	Mean	SD	*P*	Mean	SD	*P*	Mean	SD	*P*	Mean	SD	*P*	Mean	SD	*P*
SMG	21–30	N/A			N/A			27.2	5.5	0.899	21.7	4.9	0.251	4.4	0.9	0.159
	31–40	N/A			N/A			29.6	7.3	0.289	26.0	7.8	0.370	5.0	1.1	0.670
	41–50							28.5	6.3	0.604	24.4	4.3	0.887	4.8	0.9	0.810
	51–60							27.4	7.1	—	24.1	8.3	—	4.9	1.3	—
MR	21–30	3.7	0.5	0.692	3.1	0.6	0.736	25.2	3.1	0.466	17.1	3.5	0.051	5.1	0.7	0.615
	31–40	3.4	0.4	0.120	3.4	0.6	0.237	25.9	3.2	0.996	21.2	4.4	0.365	5.1	0.9	0.615
	41–50	3.5	0.3	0.200	3.1	0.6	0.690	25.0	3.7	0.375	18.4	3.7	0.276	5.0	0.9	0.907
	51–60	3.6	0.4	—	3.2	0.6	—	25.9	2.6	—	19.9	5.8	—	5.0	1.0	—
IR	21–30	3.9	0.8	0.497	3.7	0.9	0.268	29.0	8.2	0.224	28.0	7.8	0.170	5.2	0.7	0.747
	31–40	3.5	0.8	0.536	3.8	0.8	0.531	26.6	6.7	0.867	30.4	6.6	0.833	5.6	1.1	0.454
	41–50	3.6	0.7	0.734	4.0	0.6	0.896	25.9	6.4	0.891	28.7	5.3	0.305	5.4	1.1	0.893
	51–60	3.7	0.7	—	4.0	0.7	—	26.2	7.2	—	30.9	6.5	—	5.3	1.1	—
LR	21–30	2.5	0.5	0.013	4.2	0.7	0.259	**20.2**	**3.5**	**<0.001**	35.0	6.0	0.008	4.2	0.9	0.393
	31–40	2.1	0.4	0.416	3.8	0.7	0.688	**17.4**	**3.8**	**0.040**	32.3	6.2	0.180	4.7	1.0	0.396
	41–50	2.4	0.6	0.236	4.0	0.9	0.595	**16.8**	**3.6**	**0.010**	32.2	7.1	0.197	4.4	1.0	0.774
	51–60	2.2	0.3	—	3.9	0.8	—	**14.6**	**2.5**	—	29.6	5.8	—	4.5	0.7	—
SO	21–30	2.6	0.6	0.180	2.0	0.6	0.519	11.7	3.0	0.339	8.4	3.4	0.333	N/A		
	31–40	2.2	0.6	0.346	2.5	0.8	0.116	9.4	3.6	0.236	10.9	4.7	0.280	N/A		
	41–50	2.4	0.5	0.840	2.2	0.6	0.681	10.2	3.5	0.702	9.8	3.5	0.837			
	51–60	2.4	0.6	—	2.1	0.7	—	10.7	3.6	—	9.6	3.7	—			
ON	21–30	5.5	0.7	0.436	4.2	0.4	0.704	28.5	5.9	0.352	17.3	2.8	0.895	N/A		
	31–40	5.3	0.7	0.828	4.1	0.5	0.177	27.0	6.6	0.886	16.5	3.4	0.416	N/A		
	41–50	5.4	0.8	0.714	4.2	0.5	0.471	28.3	7.3	0.401	17.5	2.7	0.764			
	51–60	5.4	0.6	—	4.3	0.5	—	26.7	4.4	—	17.2	2.8	—			

Bold type indicates statistical significance.

TABLE 4. Normative Measurements of the Orbital Structures in Different Populations

	Our Study (n = 80)						Turkish MRI Study[16] (n = 100)		Turkish CT Study[17] (n = 100)		Korean CT Study[20] (n = 100)	
	at 0 mm		at 7 mm		Maximal							
Parameter	Mean	Normal Range	Mean	Normal Range	Mean	Normal Range	Mean	Normal Range	Mean	Normal Range	Mean	Normal Range
SMG	N/A	N/A	N/A	N/A	4.8	2.6–7.0	4.4	3.1–5.6	4.6	3.2–6.1	4.0	2.6–5.4
MR	3.6	2.8–4.4	3.2	2.0–4.4	5.1	3.3–6.9	4.0	3.2–4.9	4.2	3.3–5.0	3.7	3.2–5.2
IR	3.7	2.1–5.3	3.9	2.3–5.5	5.4	3.4–7.4	4.8	3.7–6.0	4.8	3.2–6.5	4.1	2.5–5.7
LR	2.3	1.3–3.3	4.0	2.4–5.6	4.5	2.7–6.3	3.7	2.6–4.8	3.3	1.7–4.8	3.4	2.1–4.7
SO	2.4	1.2–3.6	2.2	0.8–3.6	N/A	N/A	N/A	N/A	N/A	N/A	N/A	N/A
ON	5.4	4.0–6.8	4.2	3.2–5.2	N/A	N/A	4.4	3.4–5.5	4.4	3.2–5.6	4.2	3.6–4.8

DISCUSSION

Ultrasound, CT, and MRI have been widely used in orbital imaging. With high soft tissue contrast, multiplanar imaging capability, and lack of ionization radiation, MRI is the ideal modality for serial monitoring of orbital soft tissue structures. The normal MRI anatomy of the orbit has been well published,[21–23] but normative data on orbital MRI measurements are limited, especially for the Asian/Chinese population.

In this study, our orbital scans were performed at a higher magnetic field (3T) than the conventional MRI systems (0.5–1.5T) used in the literature. Higher magnetic fields (3–4T) have been shown to provide better signal-to-noise ratio (SNR) with higher spatial resolution for more accurate morphometric analysis. Another advantage of higher magnetic field is the reduction in image-acquisition time, which in turn reduces possible motion artifact.[24]

Other precautions that we took in this study to obtain better image quality and analysis include the use of fixation target to control motion artifact and asymmetrical muscle contraction; the use of a surface coil to improve SNR and to provide a smaller field of view with higher resolution; 1-mm contiguous (no gap) image acquisition for higher resolution multiplanar reconstruction; quasisagittal planes for assessment of the whole muscle (SMG and IR) at a glance in their natural course, avoiding the alignment problems that are encountered in the sagittal view; a check of inter- and intraobserver variability to ascertain the quality of the image analyses.

Unlike the earlier studies of volumetric and maximum thickness measurements[11–20] in which the image acquisition covers the whole orbit, we chose to limit our scan from equator to orbital apex for two reasons: Region-targeted image acquisition shortened the scanning time, reduced the possibility of motion artifact, and served the purpose of our study. Although the concept of volumetric measurement is appealing, it is both technically challenging and time consuming. Moreover, despite the advances, accurate measurement of the EOMs is still limited by the poor differentiation of soft tissue structures on MRI (e.g., the LPS and SR, the IR and the infraorbital neurovascular bundle, muscles and their tendon insertions, and origin of the recti at the orbital apex).

We have reported the measurements from both the preselected coronal slices and the more popular maximum thickness of the axial and quasisagittal planes in this study. Although the preselected coronal slices may or may not intersect the muscles at their maximum diameter, its diameter and cross-sectional area measurement were shown to correlate well with muscle volume.[15] Moreover, the coronal view is readily available in any ordinary MRI scan and it is the only plane in which clinicians can assess all four recti and superior oblique at a glance. Our coronal measurements data are more easily applicable to clinicians then data from the earlier studies.

The lack of consistent association between EOM measurements and demographic factors was similar to that previously reported in the literature.[17,18,20] Besides the fact that our sample size was limited, age and sex were probably poor markers for EOM morphometric analysis in the adult age group. In future research, we will look into the association between EOM measurements and anthropometric parameters (e.g., head circumference and interzygomatic distance).

With computer-assisted segmentation from original DICOM data, the imaging analysis was more direct, objective, accurate, reproducible, and reliable than was tracing projected image and digitalized information in the earlier studies. As a result, high ICCs for inter- and intraobserver reliability were expected. The relatively weaker ICCs in the IR measurements were because of the difficulty in clearly differentiating IRs from the neurovascular bundle during image analysis.

TABLE 5. Comparison of Chinese Normative Measurements and Pathologic Values in TO

	Our Study (n = 80)						TO[15] (n = 70)	
	at 0 mm		at 7 mm		Maximal			
Parameter	Mean	Normal Range	Mean	Normal Range	Mean	Normal Range	Mean	Normal Range
SMG	N/A	N/A	N/A	N/A	4.8	2.6–7.0	5.1	3.8–6.0
MR	3.6	2.8–4.4	3.2	2.0–4.4	5.1	3.3–6.9	4.5	4.0–5.6
IR	3.7	2.1–5.3	3.9	2.3–5.5	5.4	3.4–7.4	6.9	5.0–8.1
LR	2.3	1.3–3.3	4.0	2.4–5.6	4.5	2.7–6.3	4.1	3.3–5.0
SO	2.4	1.2–3.6	2.2	0.8–3.6	N/A	N/A	N/A	N/A
ON	5.4	4.0–6.8	4.2	3.2–5.2	N/A	N/A	4.4	3.4–5.5

The measurements of EOMs and ON in our study were comparable to those reported in the literature (Table 4). Our data had a relatively wide SD compared with data in other studies of similar scale. We do not know whether this observation is related to our study population or is a unique feature among the Chinese. We hope more published data will be available in the future.

Currently, there is no large-scale radiologic study of orbital diseases in the Chinese, and so pathologic values for this population are still lacking. We have included the pathologic values of thyroid orbitopathy from other population for comparison (Table 5). This study was part of a larger trial, and we are taking this opportunity to establish the baseline for further reference.

Conclusion

The 3T MRI–derived normative measurements of Chinese EOMs and ON are reproducible, comparable with those published in the literature, and can be useful in assessing diseases of the EOMs in the Chinese population.

References

1. Hosten N, Sander B, Cordes M, et al. Graves ophthalmopathy: MR imaging of the orbits. *Radiology.* 1989;172:759–762.
2. Ohnishi T, Noguchi S, Murakami N, et al. Extraocular muscles in Graves ophthalmopathy: usefulness of T2 relaxation time measurements. *Radiology.* 1994;190:857–862.
3. Yokoyama N, Nagataki S, Uetani M, et al. Role of magnetic resonance imaging in the assessment of disease activity in thyroid-associated ophthalmopathy. *Thyroid.* 2002;12:223–227.
4. Mayer EJ, Fox DL, Herdman G, et al. Signal intensity, clinical activity and cross-sectional areas on MRI scans in thyroid eye disease. *Eur J Radiol.* 2005;56:20–24.
5. Laitt RD, Hoh B, Wakeley C, et al. The value of short tau inversion recovery sequence in magnetic resonance imaging of thyroid eye disease. *Br J Radiol.* 1994;67:244–247.
6. Hoh HB, Laitt RD, Wakeley C, et al. The STIR sequence MRI in the assessment of extraocular muscles in thyroid eye disease. *Eye.* 1994;8:506–510.
7. Mayer E, Herdman G, Burnett C, et al. Serial STIR magnetic resonance imaging correlates with clinical score of activity in thyroid eye disease. *Eye.* 2001;15:313–318.
8. Taoka T, Iwasaki S, Uchida H, et al. Enhancement pattern of normal extraocular muscles in dynamic contrast-enhanced MR imaging with fat suppression. *Acta Radiol.* 2000;41:211–216.
9. Toaka T, Sakamoto M, Nakagawa H, et al. Evaluation of extraocular muscles using dynamic contrast enhanced MRI in patients with chronic thyroid orbitopathy. *J Comp Assist Tomogr.* 2005;29:115–120.
10. Ott M, Breiter N, Albrecht CF, et al. Can contrast enhanced MRI predict the response of Graves' ophthalmopathy to orbital radiotherapy? *Br J Radiol.* 2002;75:514–517.
11. Firbank MJ, Coulthard A. Evaluation of a technique for estimation of extraocular muscle volume using 2D MRI. *Br J Radiol.* 2000; 73:1282–1289.
12. Majos A, Grzelak P, Mlynarczyk W, et al. Eyeball muscles' diameters versus volume estimated by numerical image segmentation. *Eur J Ophthalmol.* 2007;17:1–6.
13. Nishida Y, Tian S, Isberg B, et al. MRI measurements of orbital tissues in dysthyroid ophthalmopathy. *Graefes Arch Clin Exp Ophthalmol.* 2001;239:824–831.
14. Kvetny J, Puhakka KB, Rohl L. Magnetic resonance imaging determination of extraocular eye muscle volume in patients with thyroid-associated ophthalmopathy and proptosis. *Acta Ophthalmol Scand.* 2006;84:419–423.
15. Szucs-Farkas Z, Toth J, Balazs E, et al. Using morphologic parameters of extraocular muscles for diagnosis and follow-up of Graves' ophthalmopathy: Diameters, areas or volumes? *AJR Am J Roentgenol.* 2002;179:1005–1010.
16. Bijlsma WR, Mourits MP. Radiologic measurement of extraocular muscle volumes in patients with Graves' orbitopathy: A review and guideline. *Orbit.* 2006;25:83–91.
17. Ozgen A, Ariyurek M. Normative measurement of orbital structures using CT. *AJR Am J Roentgenol.* 1998;170:1093–1096.
18. Ozgen A, Aydingoz U. Normative measurement of orbital structures using MRI. *J Comp Assist Tomogr.* 2000;24:493–496.
19. Tian S, Nishida Y, Isberg B, Lennerstrand G. MRI measurements of normal extraocular muscles and other orbital structures. *Graefes Arch Clin Exp Ophthalmol.* 2000;238:393–404.
20. Lee JS, Lim DW, Lee SH, et al. Normative measurements of Korean orbital structures revealed by computerized tomography. *Acta Ophthalmol. Scand.* 2001;79:197–200.
21. DePotter P, Shields JA, Shields C. *MRI of the Eye and Orbit*. Philadelphia: Lippincott; 1995.
22. Langer B, Mafee MF, Pollack S, et al. MRI of the normal orbit and optic pathway. *Radiol Clin North Am.* 1987;25:429–446.
23. Ettl A, Kramer J, Daxer A, Koornneef L. High-resolution magnetic resonance imaging of the normal extraocular musculature. *Eye.* 1997;11:793–797.
24. Takahashi M, Uematsu H, Hatabu H. MR imaging at high magnetic fields. *EJR.* 2003;46:45–52.